Study of excited Ξ states in $\psi(3686) \to K^-\Lambda\bar{\Xi}^+ + \mathrm{c.c.}$

M. Ablikim *et al.*[*]
(BESIII Collaboration)

(Received 30 August 2023; accepted 29 February 2024; published 16 April 2024)

Based on a sample of $(448.1 \pm 2.9) \times 10^6$ $\psi(3686)$ events collected with the BESIII detector at BEPCII, the decays of $\psi(3686) \to K^-\Lambda\bar{\Xi}^+ + \mathrm{c.c.}$ with $\bar{\Xi}^+ \to \bar{\Lambda}\pi^+$, $\bar{\Lambda} \to \bar{p}\pi^+$ are studied. We investigate the two excited resonances, $\Xi(1690)^-$ and $\Xi(1820)^-$, which are each observed with large significance ($\gg 10\sigma$) in the $K^-\Lambda$ invariant mass distributions. A partial wave analysis is performed, and the spin-parities of $\Xi(1690)^-$ and $\Xi(1820)^-$ are measured to be $\frac{1}{2}^-$ and $\frac{3}{2}^-$, respectively. The masses, widths, and product branching fractions of $\Xi(1690)^-$ and $\Xi(1820)^-$ are also measured.

DOI: 10.1103/PhysRevD.109.072008

I. INTRODUCTION

In the quark model [1], hadrons are viewed as composite objects of constituent spin-$\frac{1}{2}$ quarks bound by the strong interaction. Mesons are made of quark-antiquark ($q\bar{q}$) pairs and baryons are made of three quarks (qqq). Within this simple quark model, the qualitative properties of hadrons and the phenomenology of meson and baryon spectroscopy are well-explained. The accepted full theory of the strong interaction is quantum chromodynamics (QCD), a non-Abelian gauge-field theory that describes the interactions of quarks and gluons and has the features of asymptotic freedom and confinement of quarks. The understanding of the quark-gluon structure of baryons is one of the most important tasks in both particle and nuclear physics. Since baryons represent the simplest system in which the three colors of QCD neutralize into colorless objects and the essential non-Abelian character of QCD is manifested, systematic study of baryon spectroscopy can provide critical insights into the nature of QCD in the confinement domain.

The mass spectra, together with their production and decay rates, provide the main sources of information to study their structure. Much experimental work has been dedicated to the study of baryon spectroscopy. However, the available experimental information for strange baryons remains very incomplete. In particular, we are lacking knowledge of the excited baryon states with two strange quarks, i.e., Ξ^* hyperons, due to their small production cross sections and the complicated topology of the final states. Some phenomenological QCD-inspired models predict more than thirty such kinds of hyperons, however, only about a dozen total Ξ states have been observed to date. Among them, only a few are well established with spin-parity determined. The spin of $\Xi(1820)$ is determined to be $\frac{3}{2}$ [2] and the corresponding parity is measured to be negative [3]. Some evidence that the $\Xi(1690)$ has $J^P = \frac{1}{2}^-$ was found in a study of $\Lambda_c^+ \to \Xi^-\pi^+K^+$ [4].

In recent years, charmonium data samples with unprecedented statistics were accumulated by the Beijing Spectrometer (BESIII [5]) at the Beijing Electron-Positron Collider (BEPCII [6]), and these provide great opportunities for investigating the light baryons produced in charmonium decays. In a previous analysis using a sample of 106×10^6 $\psi(3686)$ events collected with BESIII, two hyperons, $\Xi(1690)^-$ and $\Xi(1820)^-$, were observed in the $K^-\Lambda$ invariant mass distribution [7]. Now, with four times more $\psi(3686)$ events collected at BESIII, we conduct a more extensive study of the decays $\psi(3686) \to K^-\Lambda\bar{\Xi}^+ + \mathrm{c.c.}$ In particular, we perform a partial wave analysis (PWA) to study the properties of intermediate state Ξ^* hyperons.

In this paper, we report a PWA analysis of $\psi(3686) \to K^-\Lambda\bar{\Xi}^+ + \mathrm{c.c.}$, with a sample of $(448.1 \pm 2.9) \times 10^6$ $\psi(3686)$ events collected at BESIII. In the following, the charge conjugate channel is always implied.

II. BESIII DETECTOR

The BESIII detector records symmetric e^+e^- collisions provided by the BEPCII storage ring, which operates in the center-of-mass energy range from 2.0 to 4.95 GeV. BESIII has collected large data samples in this energy region [8]. The cylindrical core of the BESIII detector covers 93% of the full solid angle and consists of a helium-based multilayer drift chamber (MDC), a plastic scintillator time-of-flight system (TOF), and a CsI(Tl) electromagnetic

[*]Full author list given at the end of the article.

calorimeter (EMC), which are all enclosed in a superconducting solenoidal magnet providing a 1.0 T (0.9 T in 2012) magnetic field. The solenoid is supported by an octagonal flux-return yoke with resistive plate counter muon identification modules interleaved with steel. The charged-particle momentum resolution at $1\ \mathrm{GeV}/c$ is 0.5%, and the dE/dx resolution is 6% for electrons from Bhabha scattering. The EMC measures photon energies with a resolution of 2.5% (5%) at 1 GeV in the barrel (end cap) region. The time resolution of the TOF in the barrel region is 68 ps while that in the end cap region is 110 ps.

III. DATASETS AND MONTE CARLO SAMPLES

This study uses $(448.1 \pm 2.9) \times 10^6$ $\psi(3686)$ events collected by the BESIII detector at BEPCII in 2009 ($(107.0 \pm 0.8) \times 10^6$ events) and 2012 ($(341.1 \pm 2.1) \times 10^6$ events, taken with 0.9 T magnetic field) [9].

A GEANT4-based [10] Monte Carlo (MC) simulation software BOOST [11], which includes a geometric and material description [12] of the BESIII detector, detector response and digitization models as well as tracking of the detector running conditions and performance, is used to generate MC simulated data samples. An exclusive MC sample for the process $\psi(3686) \to K^- \Lambda \bar{\Xi}^+$, is generated to optimize the selection criteria and estimate the corresponding selection efficiency. The production of the $\psi(3686)$ is simulated by the generator KKMC [13], and the subsequent decays are generated with BesEvtGen [14,15]. An inclusive MC sample, consisting of 448×10^6 $\psi(3686)$ events, is used to study potential backgrounds. The known decay modes of the $\psi(3686)$ are generated by BesEvtGen with branching fractions set to world average values [16], and the remaining unknown decay modes are modeled by LUNDCHARM [17,18].

IV. EVENT SELECTION

Considering the full decay chain of $\psi(3686) \to K^- \Lambda \bar{\Xi}^+$ as reconstructed from the decays $\Lambda \to p\pi^-$, $\bar{\Xi}^+ \to \bar{\Lambda}\pi^+$ and $\bar{\Lambda} \to \bar{p}\pi^+$, there are six charged tracks with low momentum in the final state, and the detection efficiency is very low. Therefore a partial reconstruction method is adopted to obtain higher statistics by not requiring the prompt Λ from the $\psi(3686)$ decay. Following the K^- and $\bar{\Xi}^+$ reconstruction, the Λ four-momentum is calculated from the recoil of the $K^- \bar{\Xi}^+$ system.

With the partial reconstruction method, at least four charged tracks are required. The polar angles θ, defined with respect to the axis of the MDC, of all charged tracks is required to satisfy $|\cos\theta| < 0.93$. For the kaon, the point of closest approach to the beam line is required to be within ± 10 cm in the beam direction and 2 cm in the plane perpendicular to the beam. Since the $\bar{\Xi}^+$ particle has a displaced decay vertex, looser requirements are imposed on the charged tracks from the $\bar{\Xi}^+$ decay: the point of closest approach to the beam line of is only required to be within ± 15 cm in the beam direction and 10 cm in the plane perpendicular to the beam.

Particle identification (PID) for charged tracks combines measurements of the energy loss in the MDC ($\mathrm{d}E/\mathrm{d}x$) and the flight time in the TOF to form likelihoods $\mathcal{L}(h)$ ($h = p, K, \pi$) for each hadron h hypothesis. Tracks are identified as protons when the proton hypothesis has the highest likelihood [$\mathcal{L}(p) > \mathcal{L}(K)$ and $\mathcal{L}(p) > \mathcal{L}(\pi)$], while charged kaons and pions are identified by comparing the likelihoods for the kaon and pion hypotheses, $\mathcal{L}(K) > \mathcal{L}(\pi)$ and $\mathcal{L}(\pi) > \mathcal{L}(K)$, respectively. In this analysis, two negatively charged tracks are required to be identified as K^- and $\bar{p}$, and two positively charged tracks as pions.

The candidate $\bar{\Xi}^+$ baryon is reconstructed in two steps. A $\bar{p}\pi^+$ pair sharing a common vertex is selected to reconstruct the $\bar{\Lambda}$ candidate via a secondary vertex fit. The $\bar{\Xi}^+$ is then reconstructed with the $\bar{\Lambda}$ candidate and the other π^+ by applying another secondary vertex fit. For events with more than one $\bar{\Xi}^+$ candidate, the $\bar{p}\pi^+$ combination with the minimum $|M(\bar{p}\pi^+) - M(\bar{\Lambda})|$ is selected. Here, $M(\bar{p}\pi^+)$ is the invariant mass of the $\bar{p}\pi^+$ combination, see Fig. 1(a), and $M(\bar{\Lambda})$ is the known mass of Λ taken from the Particle Data Group (PDG) [16].

A mass window of $1.110\ \mathrm{GeV}/c^2 < M(\bar{p}\pi^+) < 1.121\ \mathrm{GeV}/c^2$ is imposed to select $\bar{\Lambda}$ candidates as shown in Fig. 1(a) by the blue dashed arrows. The distribution of the $\bar{\Xi}^+$ decay length, $L(\bar{\Xi}^+)$, is shown in Fig. 1(b). The distribution of the $\bar{\Lambda}\pi^+$ invariant mass, $M(\bar{\Lambda}\pi^+)$, is shown in Fig. 1(c), after a requirement of $L(\bar{\Xi}^+) > 0.5$ cm is applied. The invariant mass $M(\bar{\Lambda}\pi^+)$ is required to satisfy $1.315\ \mathrm{GeV}/c^2 < M(\bar{\Lambda}\pi^+) < 1.330\ \mathrm{GeV}/c^2$. The distribution of the mass recoiling against K^- and the reconstructed $\bar{\Xi}^+$, $\mathrm{RM}(K^-\bar{\Xi}^+)$, is shown in Fig. 1(d). One can see a clear Λ baryon signal around $1.115\ \mathrm{GeV}/c^2$ and the main background from Σ^0 decays around $1.193\ \mathrm{GeV}/c^2$. The requirement $1.080\ \mathrm{GeV}/c^2 < \mathrm{RM}(K^-\bar{\Xi}^+) < 1.140\ \mathrm{GeV}/c^2$ is imposed to select prompt Λ candidates. In total, 1714 events are selected.

After the above selection, a one-constraint kinematic fit that constrains the mass of the missing Λ to the PDG value, is performed to improve the resolution, and no event is rejected. The distributions of $M(K^-\bar{\Xi}^+)$, $M(\Lambda\bar{\Xi}^+)$, and $M(K^-\Lambda)$ are shown in Figs. 2(b)–2(d), respectively. Two diagonal bands on the Dalitz plot as shown in Fig. 2(a) correspond to the two structures near $1.7\ \mathrm{GeV}/c^2$ and $1.8\ \mathrm{GeV}/c^2$ in the $M(K^-\Lambda)$ mass spectrum.

To investigate possible background events, the same analysis is performed to the $\psi(3686)$ inclusive MC sample, and nineteen background events are found. A detailed event type analysis with a generic tool, TopoAna [19], shows that the main background is from $\psi(3686) \to \gamma\chi_{c1,c2}, \chi_{c1,c2} \to n\bar{K}^*\bar{\Lambda} + \mathrm{c.c.}$ decays plus some other decays with $K^-\pi^+\pi^-\bar{p}$ in the final state. A sideband method is used

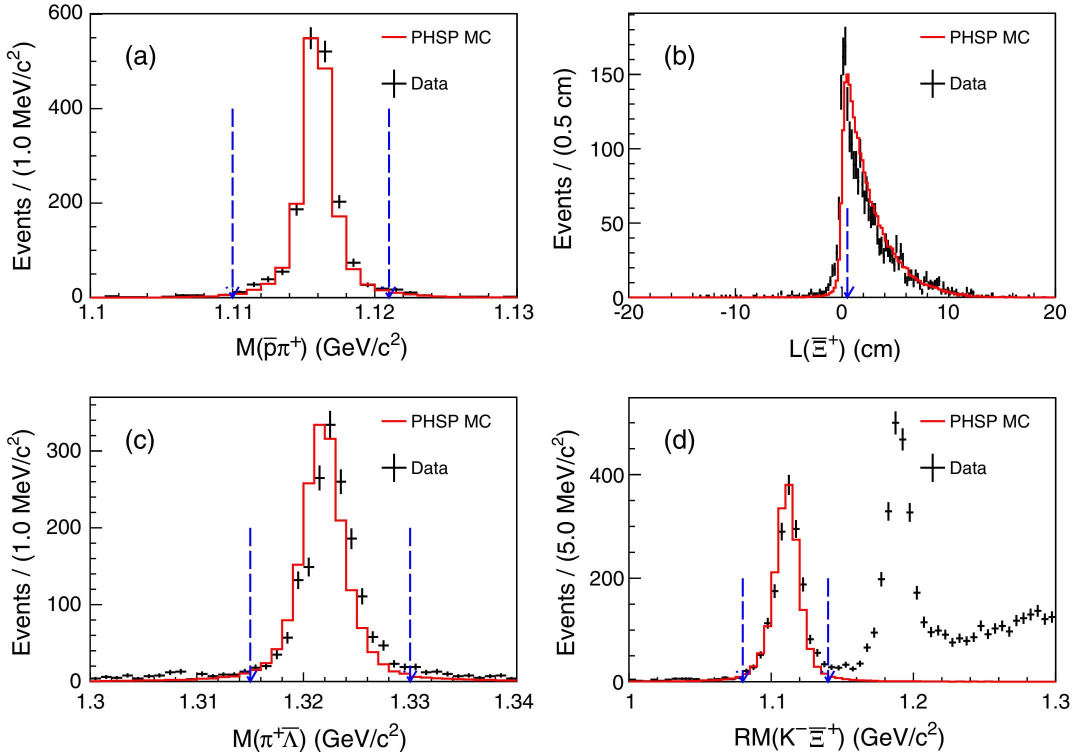

FIG. 1. Distribution of $M(\bar{p}\pi^+)$ of $\bar{\Lambda}$ candidates (a), decay length of $\bar{\Xi}^+$ candidates (b), and $M(\bar{\Lambda}\pi^+)$ of $\bar{\Xi}^+$ candidates (c). Plot (d) shows the distribution of RM$(K^-\bar{\Xi}^+)$: the left peak is Λ, while the right one is Σ^0. The crosses represent data and the histograms represent phase space (PHSP) MC. The dashed arrows show the cut values; for each plot, cuts on the other three quantities are applied.

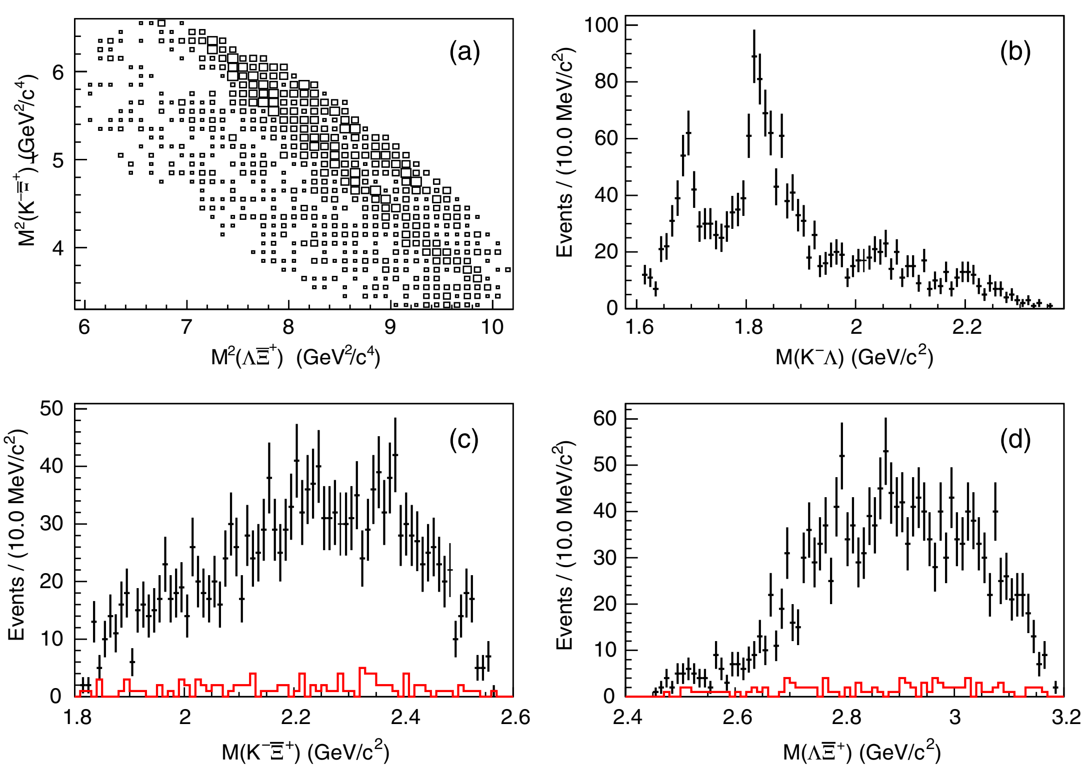

FIG. 2. (a) Dalitz plot of $M^2(\Lambda\bar{\Xi}^+)$ vs $M^2(K^-\bar{\Xi}^+)$ and the distributions of (b) $M(K^-\Lambda)$, (c) $M(K^-\bar{\Xi}^+)$ and (d) $M(\Lambda\bar{\Xi}^+)$ after the final selection. The crosses represent the data and the histograms represent the background events estimated from the Ξ sidebands.

in data to estimate the background contribution. The sideband regions of $\bar{\Xi}^+$ are defined to be (1.3025, 1.3100) and (1.3350, 1.3425) GeV$/c^2$. A total of 104 background events, corresponding to a background level of 6%, are obtained. No peaking background is observed in the recoil mass for the $\bar{\Xi}^+$ sideband events. The lower background level in the MC is attributed to the lack of simulation of the decays of higher-mass excited states and to the incomplete description of the decays of the excited states that are simulated. Additionally, the continuum data taken at a center-of-mass energy of 3.65 GeV with an integrated luminosity of 42.6 pb^{-1} is used to estimate the background from quantum electrodynamics processes, and no background event remains.

V. PARTIAL WAVE ANALYSIS

The two-body decay amplitudes in the sequential decay process $\psi(3686) \to \bar{\Xi}^+\Xi_X^{*-}, \Xi_X^{*-} \to K^-\Lambda$ are constructed using the relativistic covariant tensor amplitude formalism [20], and the maximum likelihood method is used in the PWA, with the FDC [21] package. Here, Ξ_X^{*-} denotes an intermediate state such as $\Xi(1620)^-$, $\Xi(1690)^-$, $\Xi(1830)^-$, etc.

A. Introduction to PWA

The amplitude A_j for the jth possible partial wave in $\psi(3686) \to \bar{\Xi}^+\Xi_X^{*-}, \Xi_X^{*-} \to K^-\Lambda$ is described as

$$A_j = A^j_{\mathrm{prod},X}(BW)_X A_{\mathrm{decay},X}, \tag{1}$$

where $A^j_{\mathrm{prod},X}$ is the amplitude describing the production of the intermediate resonance Ξ_X^{*-}, BW_X is the Breit-Wigner propagator of Ξ_X^{*-}, and $A_{\mathrm{decay},X}$ is the decay amplitude of Ξ_X^{*-}.

The total differential cross section $d\sigma/d\Phi$ is

$$\frac{d\sigma}{d\Phi} = \left|\sum_j c_j A_j\right|^2, \tag{2}$$

where σ is the total cross section, Φ is the phase space, and c_j is a complex free parameter to be determined in the fit for each partial wave A_j.

The probability to observe the event characterized by the variable ξ is

$$P(\xi) = \frac{\omega(\xi)\epsilon(\xi)}{\int d\xi\omega(\xi)\epsilon(\xi)}, \tag{3}$$

where ξ are the four-momenta of the K^-, Λ, and $\bar{\Xi}^+$, $\omega(\xi) \equiv d\sigma/d\Phi$ is the probability density for a single event to populate the PHSP at ξ, and $\epsilon(\xi)$ is the detection efficiency to detect one event with ξ. The normalization integral $\int d\xi\omega(\xi)\epsilon(\xi)$ is calculated using the exclusive signal MC sample.

The likelihood for observing N events in the data sample is

$$\mathcal{L} = P(\xi_1, \xi_2, \ldots, \xi_N) = \prod_{i=1}^N P(\xi_i) = \prod_{i=1}^N \frac{\omega(\xi_i)\epsilon(\xi_i)}{\int d\xi\omega(\xi)\epsilon(\xi)}. \tag{4}$$

Rather than maximizing the likelihood function $\mathcal{L}$, the quantity $-\ln\mathcal{L}$ is minimized to obtain best values of the parameters c_j and the masses and widths of the resonances

$$-\ln\mathcal{L} = -\sum_{i=1}^N \ln\left(\frac{\omega(\xi_i)}{\int d\xi\omega(\xi)\epsilon(\xi)}\right) - \sum_{i=1}^N \ln\epsilon(\xi_i), \tag{5}$$

For a given dataset, the second term is a constant and has no impact on the determination of the parameters of the amplitudes or on the change of $-\ln\mathcal{L}$. So, in the fit, the $-\ln\mathcal{L}$ is defined as

$$-\ln\mathcal{L} = -\sum_{i=1}^N \ln\left(\frac{\omega(\xi_i)}{\int d\xi\omega(\xi)\epsilon(\xi)}\right). \tag{6}$$

The final log-likelihood value minimized for the data, S, is the sum of the log-likelihood values of the events in the Ξ signal region and background events in the Ξ sideband region with negative weights.

$$S = -\ln\mathcal{L}_{\mathrm{data}} + \ln\mathcal{L}_{\mathrm{bg}}. \tag{7}$$

The free parameters are optimized by FUMILI [22]. In the minimization procedure, a change in the log-likelihood of 0.5 represents one standard deviation for each parameter.

In this analysis, the Breit-Wigner resonance shape used for the Ξ^* is

$$\mathrm{BW}(s) = \frac{1}{M^2_{\Xi^*} - s_{K\Lambda} - iM_{\Xi^*}\Gamma_{\Xi^*}}, \tag{8}$$

where $s_{K\Lambda}$ is the invariant mass squared of the decay products of the Ξ^*.

Since nucleons have structure, form factors modifying the Breit-Wigner shape are needed to describe them. Different form factors have been discussed in Refs. [23,24], and the following ones are used in the fit:

$$J = \frac{1}{2}:\ F_N(s_{K\Lambda}) = \frac{\lambda_1^4}{\lambda_1^4 + (s_{K\Lambda} - M^2_{\Xi^*})^2}, \tag{9}$$

TABLE I. The optimized mass and width for each resonance, along with the fit fraction (FF) for each. Here, the uncertainties are statistical only.

Resonance	J^P	M (MeV/c^2)	Γ (MeV)	σ	FF
$\Xi(1690)^-$	$1/2^-$	1685^{+3}_{-3}	81^{+10}_{-9}	10.8	29.0
$\Xi(1820)^-$	$3/2^-$	1821^{+2}_{-3}	73^{+6}_{-5}	18.3	48.0
Non-res	$1/2^+$	⋯	⋯	>30	23.0

$$J = \frac{3}{2}, \frac{5}{2}: \quad F_N(s_{K\Lambda}) = e^{\frac{-|s_{K\Lambda} - M^2_{\Xi^*}|}{\lambda_2^2}}, \tag{10}$$

where J is the spin, and the cutoff parameters λ_1 and λ_2 are set to be 2.0 GeV.

B. PWA results

According to the $M(K^-\bar{\Xi}^+)$, $M(\Lambda\bar{\Xi}^+)$, and $M(K^-\Lambda)$ spectra, as shown in Fig. 2, no significant enhancement is observed except the two structures near 1.7 GeV/c^2 and 1.8 GeV/c^2 in the $M(K^-\Lambda)$ spectrum. In the PWA, there are seven PDG-listed candidate Ξ hyperons, $\Xi(1620)^-$, $\Xi(1690)^-$, $\Xi(1820)^-$, $\Xi(1950)^-$, $\Xi(2030)^-$, $\Xi(2120)^-$ and $\Xi(2250)^-$. A coherent non-resonant contribution is also considered, denoted as non-res, which is described as a wide intermediate state with certain spin-parity.

1. Nominal fit

In the first step of partial wave analysis, all possible sets of amplitudes corresponding to the seven PDG-listed candidate Ξ hyperons are evaluated. The masses and widths of resonances are fixed to the PDG. The significance for a resonance is calculated based on the improvement in PWA quality, ΔS, with the change in degrees of freedom considered. Only the $\Xi(1690)^-$ and $\Xi(1820)^-$ have significances greater than 5σ. The other five Ξ resonances tested ($\Xi(1620)^-$, $\Xi(1950)^-$, $\Xi(2030)^-$, $\Xi(2120)^-$, and $\Xi(2250)^-$), each with significance less than 5σ, are excluded from the nominal fit. Each was tried with a variety of J^P values: $1/2^\pm, 3/2^\pm, 5/2^\pm, 7/2^\pm$. Their impact will be considered as a systematic uncertainty. The J^P of Ξ(1690) and Ξ(1820) are favored to be $\frac{1}{2}^-$ and $\frac{3}{2}^-$, respectively.

In the next step, the masses and widths of Ξ(1690) and Ξ(1820) are further optimized. The obtained results are shown in Table I. The masses and widths of $\Xi(1690)^-$ and $\Xi(1820)^-$ are consistent with the PDG values within 2.6σ.

The projections on the $M(K^-\bar{\Xi}^+)$, $M(\Lambda\bar{\Xi}^+)$, $M(K^-\Lambda)$ spectra after PWA are shown in Fig. 3. They agree with those of the data. We observe 464 ± 43 $\Xi(1690)^-$ events with a mass $M = 1685^{+3}_{-3}$ MeV/c^2 and a width $\Gamma = 81^{+10}_{-9}$ MeV, and 776 ± 42 $\Xi(1820)^-$ events with a mass $M = 1821^{+2}_{-3}$ MeV/c^2 and a width $\Gamma = 73^{+6}_{-5}$ MeV. Here, the uncertainties are statistical only. The statistical significances of both structures are greater than 10σ. These significances as well as the fit fractions are given in Table I.

2. Check of the nominal fit

Different J^P assignments for the nominal fit have been tested as shown in Table II. The likelihood values become worse with respect to that of the nominal fit.

The other possible non-resonant contributions in the $\Lambda\bar{\Xi}^+$ and $K^-\bar{\Xi}^+$ systems are investigated by replacing $1/2^-$ non-res → $K^-\Lambda$ in the nominal fit. As shown in Table III, the likelihood values also become worse.

3. Branching fractions

To determine the detection efficiencies of $\psi(3686) \to \Xi(1690)^-\bar{\Xi}^+$ and $\psi(3686) \to \Xi(1820)^-\bar{\Xi}^+$, signal MC events are generated using the PWA amplitude for each process. The product branching fraction of $\psi(3686) \to \bar{\Xi}^+\Xi^{*-}(\Xi^{*-} \to K^-\Lambda)$ + c.c. is calculated with

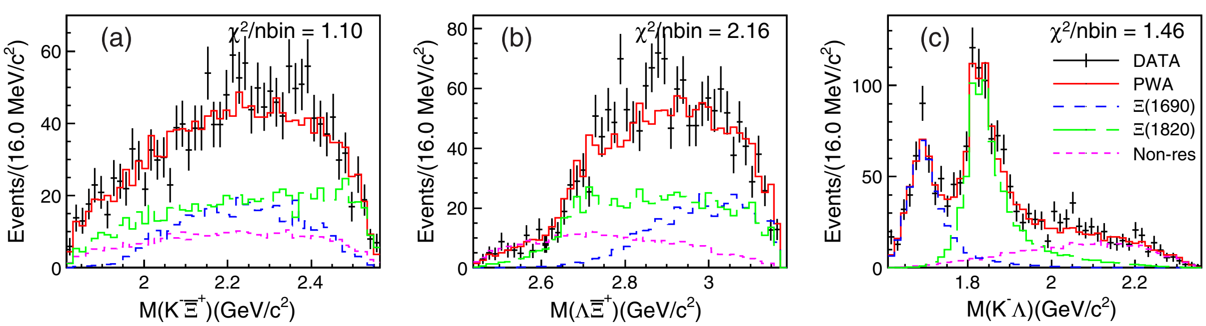

FIG. 3. Distributions of (a) $M(K^-\bar{\Xi}^+)$, (b) $M(\Lambda\bar{\Xi}^+)$, and (c) $M(K^-\Lambda)$. The crosses represent data and red solid histograms represent the projection of the PWA result. The different color histograms represent the intensity of each component in the nominal fit. Here, χ^2/nbin demonstrates the goodness of fit in each figure, where nbin is the number of bins in each figure and χ^2 is defined as $\chi^2 = \sum_{i=1}^{\text{nbin}} (n_i - v_i)^2/v_i$, where n_i and v_i are the numbers of events for the data and the fit projections of the nominal fit in the ith interval of each figure, respectively.

TABLE II. The checks of different J^P assignments. ΔS is the change of S compared to the nominal fit.

J^P	Non-res $\to K^-\Lambda$	$\Xi(1690)^-$	$\Xi(1820)^-$
$1/2^-$	53.3	$\cdots$	11.2
$1/2^+$	$\cdots$	29.2	12.6
$3/2^-$	44.9	110.6	$\cdots$
$3/2^+$	7.7	33.6	13.9

TABLE III. The checks of other possible non-resonant contributions.

Non-res process	J^P	ΔS
Non-res $\to K^-\Lambda$	$1/2^-$	53.3
Non-res $\to \Lambda\bar{\Xi}^+$	0^-	43.9
	1^-	14.8
	1^+	22.3
Non-res $\to K^-\bar{\Xi}^+$	$1/2^-$	8.8
	$1/2^+$	33.9

$$\mathcal{B}(\psi(3686)\to\bar{\Xi}^+\Xi^{*-}+\text{c.c.})\cdot\mathcal{B}(\Xi^{*-}\to K^-\Lambda) = \frac{N_{\Xi^*}}{N_{\psi(3686)}\cdot\mathcal{B}(\bar{\Xi}^+\to\bar{\Lambda}\pi^+)\cdot\mathcal{B}(\bar{\Lambda}\to\bar{p}\pi^+)\cdot\epsilon_{\Xi^*}}, \quad (11)$$

where N_{Ξ^*} is the number of $\psi(3686)\to\Xi^{*-}\bar{\Xi}^+ + \text{c.c.}$ events, $N_{\psi(3686)} = (448.1\pm 2.9)\times 10^6$ is the total number of $\psi(3686)$ events [25], and $\mathcal{B}(\bar{\Lambda}\to\bar{p}\pi^+)$ and $\mathcal{B}(\bar{\Xi}^+\to\bar{\Lambda}\pi^+)$ are the corresponding decay branching fractions [16]. The detection efficiency is $\epsilon_{\Xi^*} = 16.0\%$ for $\Xi(1690)^-$, and the corresponding product branching fraction is $(1.06\pm 0.10)\times 10^{-5}$. Similarly, the product branching fraction for $\Xi(1820)^-$ is $(1.78\pm 0.10)\times 10^{-5}$ with a detection efficiency $\epsilon_{\Xi^*} = 14.6\%$.

Fitting the $\text{RM}(K^-\bar{\Xi}^+)$ distribution, shown in Fig. 4, yields the number of signal events of $\psi(3686)\to K^-\Lambda\bar{\Xi}^+$ as $N_{\text{sig}} = 1572\pm 45$. The signal is modeled by a signal MC shape of Λ convolved with a Gaussian function while the background components from Σ^0 and χ_{cJ} are described by the MC shapes, and other background channels are described with a third order polynomial function. The branching fraction of this decay is determined to be

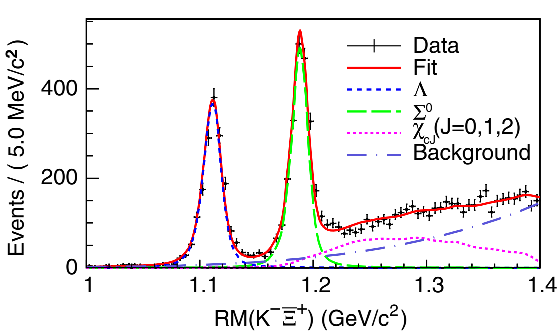

FIG. 4. Fit to the $\text{RM}(K^-\bar{\Xi}^+)$ distribution. The crosses are data and the red curve denotes the best fit. The other curves show the different fit components listed in the legend.

$$\mathcal{B}(\psi(3686)\to K^-\Lambda\bar{\Xi}^+ + \text{c.c.}) = \frac{N_{\text{sig}}}{N_{\psi(3686)}\cdot\mathcal{B}(\bar{\Xi}^+\to\bar{\Lambda}\pi^+)\cdot\mathcal{B}(\bar{\Lambda}\to\bar{p}\pi^+)\cdot\epsilon} = (3.60\pm 0.10)\times 10^{-5}. \quad (12)$$

Here, $\epsilon = 15.3\%$ is the detection efficiency for the final state. It is studied with the exclusive signal MC events which are generated using the PWA results obtained in this analysis. The uncertainty is statistical only.

VI. SYSTEMATIC UNCERTAINTIES

In this analysis, the sources of the systematic uncertainty are classified into two categories: the uncertainty from event selection and the uncertainty from the PWA procedure. The former affects the measurement of branching fractions, while the latter affects the measurements of masses and widths of the resonances and the branching fractions of the intermediate resonances. The different sources of systematic uncertainty are discussed below.

We begin with the systematic uncertainty from event selection:

(i) The total number of $\psi(3686)$ events is obtained by studying inclusive hadronic $\psi(3686)$ decays, giving a total uncertainty of 0.65% [25]. This uncertainty is taken as a systematic uncertainty for this analysis.

(ii) The uncertainties of kaon tracking and PID efficiencies are estimated using the control sample of $J/\psi\to K_S^0 K^*$. The difference between MC and data, 1.0%, is taken as the systematic uncertainty of the tracking or PID efficiency.

(iii) The $\bar{\Xi}^+$ reconstruction efficiency is studied with the control sample of $J/\psi\to\Xi^-\bar{\Xi}^+$ [26]. The difference between MC and data, 6.6%, is taken as the systematic uncertainty and it includes the systematic uncertainties of MDC tracking and PID efficiencies for the $\bar{p}$ and both π^+.

(iv) In the fit to the $\text{RM}(K^-\bar{\Xi}^+)$ distribution, we consider three sources of uncertainty: the signal model, the background model, and the fit range. The signal model is changed to a double Gaussian function and the background model is changed to a second-order polynomial function. In both cases, the change of the result is taken as the systematic uncertainty. The fit range is also changed to different values and the maximum change of the result is taken as the uncertainty. The total systematic uncertainty from

TABLE IV. Relative systematic uncertainties (in %) on the branching fraction measurement of $\psi(3686) \to K^-\Lambda\bar{\Xi}^+ + \text{c.c.}$

Source	Uncertainty (%)
Number of $\psi(3686)$ events	0.7
MDC tracking of K^-	1.0
PID of K^-	1.0
$\bar{\Xi}^+$ reconstruction	6.6
Signal model	0.8
Background shape	0.1
Fit range	0.3
Total	6.8

fitting is the sum in quadrature of the three contributions.

The second category is the systematic uncertainty from the PWA procedure:

(i) In this analysis, the background is estimated from the $\bar{\Xi}^+$ sideband events in data. We change the background level by $\pm 1\sigma$ and redo the PWA fit. We also change the sideband range by $\pm 1\sigma$ and redo the PWA fit. For each variation, we take the difference as the associated systematic uncertainty.

(ii) We replace the non-res component in the nominal fit by the other two processes (non-res $\to \Lambda\bar{\Xi}^+$ and non-res $\to K^-\bar{\Xi}^+$) and redo the PWA fit. The differences are taken as the systematic uncertainty.

(iii) Besides $\Xi(1690)^-$ and $\Xi(1820)^-$ in the nominal fit, each known possible resonance has been included in the fit. Among them, $\Xi(1620)^-$ is the most significant one with a statistical significance of 3σ. The difference between the fit results with and without $\Xi(1620)^-$ is taken as the systematic uncertainty due to possible additional resonances.

(iv) The systematic uncertainty associated with a change of the parameters λ_1 and λ_2 is evaluated by fixing λ_2 to 2.0 GeV and varying λ_1 between 1.5 GeV and 3.0 GeV. The maximum difference to the nominal result is taken as the systematic uncertainty.

(v) In analysis, the branching fractions are obtained with the optimized masses and widths of $\Xi(1690)$ and $\Xi(1820)$. Alternatively, the branching fractions are obtained with the masses and widths of $\Xi(1690)$ and $\Xi(1820)$ fixed to the PDG values. The resulting changes in the measurements of branching fraction are assigned as systematic uncertainties.

(vi) The systematic uncertainty from fit bias is evaluated by applying nominal analysis procedure to signal MC samples generated according to the PWA results from data. The difference between input and output values is taken as the systematic uncertainty.

The two categories of systematic uncertainties are listed in Table IV and Table V.

VII. SUMMARY AND DISCUSSION

Based on $(448.1 \pm 2.9) \times 10^6$ $\psi(3686)$ events collected with the BESIII detector at BEPCII in 2009 and 2012, we report the results of a partial wave analysis of $\psi(3686) \to K^-\Lambda\bar{\Xi}^+ + \text{c.c.}$ Two excited hyperons, $\Xi(1690)^-$ and $\Xi(1820)^-$, are observed in the $M(K^-\Lambda)$ and $M(K^+\bar{\Lambda})$ spectra. Their masses, widths, spin-parities, and product branching fractions are measured. The results obtained are summarized in Tables VI and VII. We note that, whereas the masses of the $\Xi(1690)^-$ and $\Xi(1820)^-$ are in agreement with previous measurements, our width values are both larger than those measurements and only marginally consistent with them. However, our analysis is the first to use a PWA to include interference effects, and this might help explain the differences. The spin-parities of $\Xi(1690)^-$ and $\Xi(1820)^-$ are measured for the first time, which are consistent with the quark model. This work improves the knowledge of the excited hyperon spectrum. To

TABLE V. Systematic uncertainties on the measurements of the Ξ^* parameters and branching fractions.

	$\Xi(1690)$			$\Xi(1820)$		
Source	ΔM(MeV/c^2)	$\Delta\Gamma$ (MeV)	$\Delta\mathcal{B}/\mathcal{B}$(%)	ΔM (MeV/c^2)	$\Delta\Gamma$ (MeV)	$\Delta\mathcal{B}/\mathcal{B}$(%)
Number of $\psi(3686)$ events	…	…	0.7	…	…	0.7
MDC tracking of $K^\pm$	…	…	1	…	…	1
PID of $K^\pm$	…	…	1	…	…	1
$\bar{\Xi}^+$ reconstruction	…	…	6.6	…	…	6.6
Background level	0	3	1.0	1	1	0.9
Background sideband	0	4	0.4	0	1	1.4
Non-res component	11	9	11.3	2	3	15.6
Additional resonances	5	17	14.0	2	2	3.7
Different form factors	0	2	3.0	1	8	1.3
Fit bias	1	3	8.4	0	1	2.4
Resonance parameters of $\Xi(1690)$ and $\Xi(1820)$	…	…	19.8	…	…	3.2
Total	12	20	29.1	3	9	18.1

TABLE VI. Results obtained for $I(J^P)$, mass and width for each component. The first (second) uncertainty is statistical (systematic).

Resonance	$I(J^P)$	M (MeV/c^2)	Γ (MeV)
$\Xi(1690)^-$	$1/2(1/2^-)$	$1685^{+3}_{-2} \pm 12$	$81^{+10}_{-9} \pm 20$
$\Xi(1820)^-$	$1/2(3/2^-)$	$1821^{+2}_{-3} \pm 3$	$73^{+6}_{-5} \pm 9$

TABLE VII. Branching fraction results; the first (second) uncertainty is statistical (systematic).

Resonance	Branching fraction
$\mathcal{B}(\psi(3686) \to \Xi(1690)^-\bar{\Xi}^+ + \text{c.c.}) \times \mathcal{B}(\Xi(1690)^- \to K^-\Lambda)$	$(1.06 \pm 0.10 \pm 0.31) \times 10^{-5}$
$\mathcal{B}(\psi(3686) \to \Xi(1820)^-\bar{\Xi}^+ + \text{c.c.}) \times \mathcal{B}(\Xi(1820)^- \to K^-\Lambda)$	$(1.78 \pm 0.10 \pm 0.32) \times 10^{-5}$
$\psi(3686) \to K^-\Lambda\bar{\Xi}^+ + \text{c.c.}$	$(3.60 \pm 0.10 \pm 0.24) \times 10^{-5}$

understand the internal structure of baryons and test theoretical predictions, further investigations with higher statistics are needed.

ACKNOWLEDGMENTS

The BESIII Collaboration thanks the staff of BEPCII and the IHEP computing center for their strong support. This work is supported in part by National Key R&D Program of China under Contracts Nos. 2020YFA0406300, 2020YFA0406400; National Natural Science Foundation of China (NSFC) under Contracts No. 11635010, No. 11735014, No. 11835012, No. 11935015, No. 11935016, No. 11935018, No. 11961141012, No. 12022510, No. 12025502, No. 12035009, No. 12035013, No. 12061131003, No. 12075250, No. 12075252, No. 12192260, No. 12192261, No. 12192262, No. 12192263, No. 12192264, No. 12192265; the Chinese Academy of Sciences (CAS) Large-Scale Scientific Facility Program; the CAS Center for Excellence in Particle Physics (CCEPP); Joint Large-Scale Scientific Facility Funds of the NSFC and CAS under Contract No. U1832207; CAS Key Research Program of Frontier Sciences under Contracts No. QYZDJ-SSW-SLH003, No. QYZDJ-SSW-SLH040; 100 Talents Program of CAS; The Institute of Nuclear and Particle Physics (INPAC) and Shanghai Key Laboratory for Particle Physics and Cosmology; ERC under Contract No. 758462; European Union's Horizon 2020 research and innovation programme under Marie Sklodowska-Curie grant agreement under Contract No. 894790; German Research Foundation DFG under Contracts No. 443159800, No. 455635585, Collaborative Research Center CRC 1044, FOR5327, GRK 2149; Istituto Nazionale di Fisica Nucleare, Italy; Ministry of Development of Turkey under Contract No. DPT2006K-120470; National Research Foundation of Korea under Contract No. NRF-2022R1A2C1092335; National Science and Technology fund; National Science Research and Innovation Fund (NSRF) via the Program Management Unit for Human Resources & Institutional Development, Research and Innovation under Contract No. B16F640076; Polish National Science Centre under Contract No. 2019/35/O/ST2/02907; The Royal Society, UK under Contract No. DH160214; The Swedish Research Council; U.S. Department of Energy under Contract No. DE-FG02-05ER41374.

[1] M. Gell-Mann, Phys. Lett. **8**, 214 (1964).
[2] D. Teodoro *et al.*, Phys. Lett. **77B**, 451 (1978).
[3] S. F. Biagi *et al.*, Z. Phys. C **34**, 175 (1987).
[4] B. Aubert *et al.* (*BABAR* Collaboration), Phys. Rev. D **78**, 034008 (2008).
[5] M. Ablikim *et al.* (BESIII Collaboration), Nucl. Instrum. Methods Phys. Res., Sect. A **614**, 345 (2010).
[6] C. H. Yu *et al.*, *Proceedings of IPAC2016, Busan, Korea* (2016), 10.18429/JACoW-IPAC2016-TUYA01.
[7] M. Ablikim *et al.* (BESIII Collaboration), Phys. Rev. D **91**, 092006 (2015).
[8] M. Ablikim *et al.* (BESIII Collaboration), Chin. Phys. C **44**, 040001 (2020).
[9] M. Ablikim *et al.* (BESIII Collaboration), Chin. Phys. C **42**, 023001 (2018).
[10] S. Agostinelli *et al.* (GEANT4 Collaboration), Nucl. Instrum. Methods Phys. Res., Sect. A **506**, 250 (2003).

[11] Z. Y. DENG *et al.*, Chin. Phys. C **30**, 371 (2006), http://cpc.ihep.ac.cn/article/id/283d17c0-e8fa-4ad7-bfe3-92095466def1.
[12] K. X. Huang *et al.*, Nucl. Sci. Tech. **33**, 142 (2022).
[13] S. Jadach, B. Ward, and Z. Was, Comput. Phys. Commun. **130**, 260 (2000).
[14] D. Lange, Nucl. Instrum. Methods Phys. Res., Sect. A **462**, 152 (2001).
[15] R. G. Ping, Chin. Phys. C **32**, 599 (2008).
[16] R. L. Workman *et al.* (Particle Data Group), Prog. Theor. Exp. Phys. **2022**, 083C01 (2022).
[17] J. C. Chen, G. S. Huang, X. R. Qi, D. H. Zhang, and Y. S. Zhu, Phys. Rev. D **62**, 034003 (2000).
[18] R. L. Yang, R.-G. Ping, and H. Chen, Chin. Phys. Lett. **31**, 061301 (2014).
[19] X. Y. Zhou, S. X. Du, G. Li, and C. P. Shen, Comput. Phys. Commun. **258**, 107540 (2021).
[20] B. S. Zou and D. V. Bugg, Eur. Phys. J. A **16**, 537 (2003).
[21] J. X. Wang, Nucl. Instrum. Methods Phys. Res., Sect. A **534**, 241 (2004).
[22] S. N. Dymov, V. S. Kurbatov, I. N. Silin, and S. V. Yaschenko, Nucl. Instrum. Methods Phys. Res., Sect. A **440**, 431 (2000).
[23] G. Penner and U. Mosel, Phys. Rev. C **66**, 055211 (2002).
[24] W. H. Liang, P. N. Shen, B. S. Zou, and A. Faessler, Eur. Phys. J. A **21**, 487 (2004).
[25] M. Ablikim *et al.* (BESIII Collaboration), Chin. Phys. C **42**, 023001 (2018).
[26] M. Ablikim *et al.* (BESIII Collaboration), Phys. Rev. D **93**, 072003 (2016).

M. Ablikim,[1] M. N. Achasov,[13,b] P. Adlarson,[73] R. Aliberti,[34] A. Amoroso,[72a,72c] M. R. An,[38] Q. An,[69,56] Y. Bai,[55] O. Bakina,[35] I. Balossino,[29a] Y. Ban,[45,g] V. Batozskaya,[1,43] K. Begzsuren,[31] N. Berger,[34] M. Berlowski,[43] M. Bertani,[28a] D. Bettoni,[29a] F. Bianchi,[72a,72c] E. Bianco,[72a,72c] J. Bloms,[66] A. Bortone,[72a,72c] I. Boyko,[35] R. A. Briere,[5] A. Brueggemann,[66] H. Cai,[74] X. Cai,[1,56] A. Calcaterra,[28a] G. F. Cao,[1,61] N. Cao,[1,61] S. A. Cetin,[60a] J. F. Chang,[1,56] T. T. Chang,[75] W. L. Chang,[1,61] G. R. Che,[42] G. Chelkov,[35,a] C. Chen,[42] Chao Chen,[53] G. Chen,[1] H. S. Chen,[1,61] M. L. Chen,[1,56,61] S. J. Chen,[41] S. M. Chen,[59] T. Chen,[1,61] X. R. Chen,[30,61] X. T. Chen,[1,61] Y. B. Chen,[1,56] Y. Q. Chen,[33] Z. J. Chen,[25,h] W. S. Cheng,[72c] S. K. Choi,[10] X. Chu,[42] G. Cibinetto,[29a] S. C. Coen,[4] F. Cossio,[72c] J. J. Cui,[48] H. L. Dai,[1,56] J. P. Dai,[77] A. Dbeyssi,[19] R. E. de Boer,[4] D. Dedovich,[35] Z. Y. Deng,[1] A. Denig,[34] I. Denysenko,[35] M. Destefanis,[72a,72c] F. De Mori,[72a,72c] B. Ding,[64,1] X. X. Ding,[45,g] Y. Ding,[33] Y. Ding,[39] J. Dong,[1,56] L. Y. Dong,[1,61] M. Y. Dong,[1,56,61] X. Dong,[74] S. X. Du,[79] Z. H. Duan,[41] P. Egorov,[35,a] Y. L. Fan,[74] J. Fang,[1,56] S. S. Fang,[1,61] W. X. Fang,[1] Y. Fang,[1] R. Farinelli,[29a] L. Fava,[72b,72c] F. Feldbauer,[4] G. Felici,[28a] C. Q. Feng,[69,56] J. H. Feng,[57] K. Fischer,[67] M. Fritsch,[4] C. Fritzsch,[66] C. D. Fu,[1] Y. W. Fu,[1] H. Gao,[61] Y. N. Gao,[45,g] Yang Gao,[69,56] S. Garbolino,[72c] I. Garzia,[29a,29b] P. T. Ge,[74] Z. W. Ge,[41] C. Geng,[57] E. M. Gersabeck,[65] A. Gilman,[67] K. Goetzen,[14] L. Gong,[39] W. X. Gong,[1,56] W. Gradl,[34] S. Gramigna,[29a,29b] M. Greco,[72a,72c] M. H. Gu,[1,56] Y. T. Gu,[16] C. Y. Guan,[1,61] Z. L. Guan,[22] A. Q. Guo,[30,61] L. B. Guo,[40] R. P. Guo,[47] Y. P. Guo,[12,f] A. Guskov,[35,a] X. T. H.,[1,61] W. Y. Han,[38] X. Q. Hao,[20] F. A. Harris,[63] K. K. He,[53] K. L. He,[1,61] F. H. Heinsius,[4] C. H. Heinz,[34] Y. K. Heng,[1,56,61] C. Herold,[58] T. Holtmann,[4] P. C. Hong,[12,f] G. Y. Hou,[1,61] Y. R. Hou,[61] Z. L. Hou,[1] H. M. Hu,[1,61] J. F. Hu,[54,i] T. Hu,[1,56,61] Y. Hu,[1] G. S. Huang,[69,56] K. X. Huang,[57] L. Q. Huang,[30,61] X. T. Huang,[48] Y. P. Huang,[1] T. Hussain,[71] N. Hüsken,[27,34] W. Imoehl,[27] M. Irshad,[69,56] J. Jackson,[27] S. Jaeger,[4] S. Janchiv,[31] J. H. Jeong,[10] Q. Ji,[1] Q. P. Ji,[20] X. B. Ji,[1,61] X. L. Ji,[1,56] Y. Y. Ji,[48] Z. K. Jia,[69,56] P. C. Jiang,[45,g] S. S. Jiang,[38] T. J. Jiang,[17] X. S. Jiang,[1,56,61] Y. Jiang,[61] J. B. Jiao,[48] Z. Jiao,[23] S. Jin,[41] Y. Jin,[64] M. Q. Jing,[1,61] T. Johansson,[73] X. K.,[1] S. Kabana,[32] N. Kalantar-Nayestanaki,[62] X. L. Kang,[9] X. S. Kang,[39] R. Kappert,[62] M. Kavatsyuk,[62] B. C. Ke,[79] A. Khoukaz,[66] R. Kiuchi,[1] R. Kliemt,[14] L. Koch,[36] O. B. Kolcu,[60a] B. Kopf,[4] M. Kuessner,[4] A. Kupsc,[43,73] W. Kühn,[36] J. J. Lane,[65] J. S. Lange,[36] P. Larin,[19] A. Lavania,[26] L. Lavezzi,[72a,72c] T. T. Lei,[69,k] Z. H. Lei,[69,56] H. Leithoff,[34] M. Lellmann,[34] T. Lenz,[34] C. Li,[46] C. Li,[42] C. H. Li,[38] Cheng Li,[69,56] D. M. Li,[79] F. Li,[1,56] G. Li,[1] H. Li,[69,56] H. B. Li,[1,61] H. J. Li,[20] H. N. Li,[54,i] Hui Li,[42] J. R. Li,[59] J. S. Li,[57] J. W. Li,[48] Ke Li,[1] L. J. Li,[1,61] L. K. Li,[1] Lei Li,[3] M. H. Li,[42] P. R. Li,[37,j,k] S. X. Li,[12] T. Li,[48] W. D. Li,[1,61] W. G. Li,[1] X. H. Li,[69,56] X. L. Li,[48] Xiaoyu Li,[1,61] Y. G. Li,[45,g] Z. J. Li,[57] Z. X. Li,[16] Z. Y. Li,[57] C. Liang,[41] H. Liang,[69,56] H. Liang,[1,61] H. Liang,[33] Y. F. Liang,[52] Y. T. Liang,[30,61] G. R. Liao,[15] L. Z. Liao,[48] J. Libby,[26] A. Limphirat,[58] D. X. Lin,[30,61] T. Lin,[1] B. J. Liu,[1] B. X. Liu,[74] C. Liu,[33] C. X. Liu,[1] D. Liu,[19,69] F. H. Liu,[51] Fang Liu,[1] Feng Liu,[6] G. M. Liu,[54,i] H. Liu,[37,j,k] H. B. Liu,[16] H. M. Liu,[1,61] Huanhuan Liu,[1] Huihui Liu,[21] J. B. Liu,[69,56] J. L. Liu,[70] J. Y. Liu,[1,61] K. Liu,[1] K. Y. Liu,[39] Ke Liu,[22] L. Liu,[69,56] L. C. Liu,[42] Lu Liu,[42] M. H. Liu,[12,f] P. L. Liu,[1] Q. Liu,[61] S. B. Liu,[69,56] T. Liu,[12,f] W. K. Liu,[42] W. M. Liu,[69,56] X. Liu,[37,j,k] Y. Liu,[37,j,k] Y. B. Liu,[42] Z. A. Liu,[1,56,61] Z. Q. Liu,[48] X. C. Lou,[1,56,61] F. X. Lu,[57] H. J. Lu,[23] J. G. Lu,[1,56] X. L. Lu,[1] Y. Lu,[7] Y. P. Lu,[1,56] Z. H. Lu,[1,61] C. L. Luo,[40] M. X. Luo,[78] T. Luo,[12,f] X. L. Luo,[1,56] X. R. Lyu,[61] Y. F. Lyu,[42] F. C. Ma,[39] H. L. Ma,[1] J. L. Ma,[1,61] L. L. Ma,[48] M. M. Ma,[1,61] Q. M. Ma,[1] R. Q. Ma,[1,61] R. T. Ma,[61] X. Y. Ma,[1,56] Y. Ma,[45,g] F. E. Maas,[19] M. Maggiora,[72a,72c] S. Maldaner,[4] S. Malde,[67]

A. Mangoni,[28b] Y. J. Mao,[45,g] Z. P. Mao,[1] S. Marcello,[72a,72c] Z. X. Meng,[64] J. G. Messchendorp,[14,62] G. Mezzadri,[29a] H. Miao,[1,61] T. J. Min,[41] R. E. Mitchell,[27] X. H. Mo,[1,56,61] N. Yu. Muchnoi,[13,b] Y. Nefedov,[35] F. Nerling,[19,d] I. B. Nikolaev,[13,b] Z. Ning,[1,56] S. Nisar,[11,l] Y. Niu,[48] S. L. Olsen,[61] Q. Ouyang,[1,56,61] S. Pacetti,[28b,28c] X. Pan,[53] Y. Pan,[55] A. Pathak,[33] P. Patteri,[28a] Y. P. Pei,[69,56] M. Pelizaeus,[4] H. P. Peng,[69,56] K. Peters,[14,d] J. L. Ping,[40] R. G. Ping,[1,61] S. Plura,[34] S. Pogodin,[35] V. Prasad,[32] F. Z. Qi,[1] H. Qi,[69,56] H. R. Qi,[59] M. Qi,[41] T. Y. Qi,[12,f] S. Qian,[1,56] W. B. Qian,[61] C. F. Qiao,[61] J. J. Qin,[70] L. Q. Qin,[15] X. P. Qin,[12,f] X. S. Qin,[48] Z. H. Qin,[1,56] J. F. Qiu,[1] S. Q. Qu,[59] C. F. Redmer,[34] K. J. Ren,[38] A. Rivetti,[72c] V. Rodin,[62] M. Rolo,[72c] G. Rong,[1,61] Ch. Rosner,[19] S. N. Ruan,[42] N. Salone,[43] A. Sarantsev,[35,c] Y. Schelhaas,[34] K. Schönning,[73] M. Scodeggio,[29a,29b] K. Y. Shan,[12,f] W. Shan,[24] X. Y. Shan,[69,56] J. F. Shangguan,[53] L. G. Shao,[1,61] M. Shao,[69,56] C. P. Shen,[12,f] H. F. Shen,[1,61] W. H. Shen,[61] X. Y. Shen,[1,61] B. A. Shi,[61] H. C. Shi,[69,56] J. L. Shi,[12] J. Y. Shi,[1] Q. Q. Shi,[53] R. S. Shi,[1,61] X. Shi,[1,56] J. J. Song,[20] T. Z. Song,[57] W. M. Song,[33,1] Y. J. Song,[12] Y. X. Song,[45,g] S. Sosio,[72a,72c] S. Spataro,[72a,72c] F. Stieler,[34] Y. J. Su,[61] G. B. Sun,[74] G. X. Sun,[1] H. Sun,[61] H. K. Sun,[1] J. F. Sun,[20] K. Sun,[59] L. Sun,[74] S. S. Sun,[1,61] T. Sun,[1,61] W. Y. Sun,[33] Y. Sun,[9] Y. J. Sun,[69,56] Y. Z. Sun,[1] Z. T. Sun,[48] Y. X. Tan,[69,56] C. J. Tang,[52] G. Y. Tang,[1] J. Tang,[57] Y. A. Tang,[74] L. Y. Tao,[70] Q. T. Tao,[25,h] M. Tat,[67] J. X. Teng,[69,56] V. Thoren,[73] W. H. Tian,[57] W. H. Tian,[50] Y. Tian,[30,61] Z. F. Tian,[74] I. Uman,[60b] B. Wang,[1] B. L. Wang,[61] Bo Wang,[69,56] C. W. Wang,[41] D. Y. Wang,[45,g] F. Wang,[70] H. J. Wang,[37,j,k] H. P. Wang,[1,61] K. Wang,[1,56] L. L. Wang,[1] M. Wang,[48] Meng Wang,[1,61] S. Wang,[37,j,k] S. Wang,[12,f] T. Wang,[12,f] T. J. Wang,[42] W. Wang,[70] W. Wang,[57] W. H. Wang,[74] W. P. Wang,[69,56] X. Wang,[45,g] X. F. Wang,[37,j,k] X. J. Wang,[38] X. L. Wang,[12,f] Y. Wang,[59] Y. D. Wang,[44] Y. F. Wang,[1,56,61] Y. H. Wang,[46] Y. N. Wang,[44] Y. Q. Wang,[1] Yaqian Wang,[18,1] Yi Wang,[59] Z. Wang,[1,56] Z. L. Wang,[70] Z. Y. Wang,[1,61] Ziyi Wang,[61] Zongyuan Wang,[1,61] D. Wei,[68] D. H. Wei,[15] F. Weidner,[66] S. P. Wen,[1] C. W. Wenzel,[4] U. Wiedner,[4] G. Wilkinson,[67] M. Wolke,[73] L. Wollenberg,[4] C. Wu,[38] J. F. Wu,[1,61] L. H. Wu,[1] L. J. Wu,[1,61] X. Wu,[12,f] X. H. Wu,[33] Y. Wu,[69] Y. J. Wu,[30] Z. Wu,[1,56] L. Xia,[69,56] X. M. Xian,[38] T. Xiang,[45,g] D. Xiao,[37,j,k] G. Y. Xiao,[41] H. Xiao,[12,f] S. Y. Xiao,[1] Y. L. Xiao,[12,f] Z. J. Xiao,[40] C. Xie,[41] X. H. Xie,[45,g] Y. Xie,[48] Y. G. Xie,[1,56] Y. H. Xie,[6] Z. P. Xie,[69,56] T. Y. Xing,[1,61] C. F. Xu,[1,61] C. J. Xu,[57] G. F. Xu,[1] H. Y. Xu,[64] Q. J. Xu,[17] W. L. Xu,[64] X. P. Xu,[53] Y. C. Xu,[76] Z. P. Xu,[41] F. Yan,[12,f] L. Yan,[12,f] W. B. Yan,[69,56] W. C. Yan,[79] X. Q. Yan,[1] H. J. Yang,[49,e] H. L. Yang,[33] H. X. Yang,[1] Tao Yang,[1] Y. Yang,[12,f] Y. F. Yang,[42] Y. X. Yang,[1,61] Yifan Yang,[1,61] Z. W. Yang,[37,j,k] M. Ye,[1,56] M. H. Ye,[8] J. H. Yin,[1] Z. Y. You,[57] B. X. Yu,[1,56,61] C. X. Yu,[42] G. Yu,[1,61] T. Yu,[70] X. D. Yu,[45,g] C. Z. Yuan,[1,61] L. Yuan,[2] S. C. Yuan,[1] X. Q. Yuan,[1] Y. Yuan,[1,61] Z. Y. Yuan,[57] C. X. Yue,[38] A. A. Zafar,[71] F. R. Zeng,[48] X. Zeng,[12,f] Y. Zeng,[25,h] Y. J. Zeng,[1,61] X. Y. Zhai,[33] Y. H. Zhan,[57] A. Q. Zhang,[1,61] B. L. Zhang,[1,61] B. X. Zhang,[1] D. H. Zhang,[42] G. Y. Zhang,[20] H. Zhang,[69] H. H. Zhang,[57] H. H. Zhang,[33] H. Q. Zhang,[1,56,61] H. Y. Zhang,[1,56] J. J. Zhang,[50] J. L. Zhang,[75] J. Q. Zhang,[40] J. W. Zhang,[1,56,61] J. X. Zhang,[37,j,k] J. Y. Zhang,[1] J. Z. Zhang,[1,61] Jianyu Zhang,[61] Jiawei Zhang,[1,61] L. M. Zhang,[59] L. Q. Zhang,[57] Lei Zhang,[41] P. Zhang,[1] Q. Y. Zhang,[38,79] Shuihan Zhang,[1,61] Shulei Zhang,[25,h] X. D. Zhang,[44] X. M. Zhang,[1] X. Y. Zhang,[48] X. Y. Zhang,[53] Y. Zhang,[67] Y. T. Zhang,[79] Y. H. Zhang,[1,56] Yan Zhang,[69,56] Yao Zhang,[1] Z. H. Zhang,[1] Z. L. Zhang,[33] Z. Y. Zhang,[74] Z. Y. Zhang,[42] G. Zhao,[1] J. Zhao,[38] J. Y. Zhao,[1,61] J. Z. Zhao,[1,56] Lei Zhao,[69,56] Ling Zhao,[1] M. G. Zhao,[42] S. J. Zhao,[79] Y. B. Zhao,[1,56] Y. X. Zhao,[30,61] Z. G. Zhao,[69,56] A. Zhemchugov,[35,a] B. Zheng,[70] J. P. Zheng,[1,56] W. J. Zheng,[1,61] Y. H. Zheng,[61] B. Zhong,[40] X. Zhong,[57] H. Zhou,[48] L. P. Zhou,[1,61] X. Zhou,[74] X. K. Zhou,[6] X. R. Zhou,[69,56] X. Y. Zhou,[38] Y. Z. Zhou,[12,f] J. Zhu,[42] K. Zhu,[1] K. J. Zhu,[1,56,61] L. Zhu,[33] L. X. Zhu,[61] S. H. Zhu,[68] S. Q. Zhu,[41] T. J. Zhu,[12,f] W. J. Zhu,[12,f] Y. C. Zhu,[69,56] Z. A. Zhu,[1,61] J. H. Zou,[1] and J. Zu[69,56]

(BESIII Collaboration)

[1]*Institute of High Energy Physics, Beijing 100049, People's Republic of China*
[2]*Beihang University, Beijing 100191, People's Republic of China*
[3]*Beijing Institute of Petrochemical Technology, Beijing 102617, People's Republic of China*
[4]*Bochum Ruhr-University, D-44780 Bochum, Germany*
[5]*Carnegie Mellon University, Pittsburgh, Pennsylvania 15213, USA*
[6]*Central China Normal University, Wuhan 430079, People's Republic of China*
[7]*Central South University, Changsha 410083, People's Republic of China*
[8]*China Center of Advanced Science and Technology, Beijing 100190, People's Republic of China*
[9]*China University of Geosciences, Wuhan 430074, People's Republic of China*
[10]*Chung-Ang University, Seoul, 06974, Republic of Korea*
[11]*COMSATS University Islamabad, Lahore Campus, Defence Road, Off Raiwind Road, 54000 Lahore, Pakistan*

[12]Fudan University, Shanghai 200433, People's Republic of China
[13]G.I. Budker Institute of Nuclear Physics SB RAS (BINP), Novosibirsk 630090, Russia
[14]GSI Helmholtzcentre for Heavy Ion Research GmbH, D-64291 Darmstadt, Germany
[15]Guangxi Normal University, Guilin 541004, People's Republic of China
[16]Guangxi University, Nanning 530004, People's Republic of China
[17]Hangzhou Normal University, Hangzhou 310036, People's Republic of China
[18]Hebei University, Baoding 071002, People's Republic of China
[19]Helmholtz Institute Mainz, Staudinger Weg 18, D-55099 Mainz, Germany
[20]Henan Normal University, Xinxiang 453007, People's Republic of China
[21]Henan University of Science and Technology, Luoyang 471003, People's Republic of China
[22]Henan University of Technology, Zhengzhou 450001, People's Republic of China
[23]Huangshan College, Huangshan 245000, People's Republic of China
[24]Hunan Normal University, Changsha 410081, People's Republic of China
[25]Hunan University, Changsha 410082, People's Republic of China
[26]Indian Institute of Technology Madras, Chennai 600036, India
[27]Indiana University, Bloomington, Indiana 47405, USA
[28a]INFN Laboratori Nazionali di Frascati, I-00044, Frascati, Italy
[28b]INFN Sezione di Perugia, I-06100, Perugia, Italy
[28c]University of Perugia, I-06100, Perugia, Italy
[29a]INFN Sezione di Ferrara, I-44122, Ferrara, Italy
[29b]University of Ferrara, I-44122, Ferrara, Italy
[30]Institute of Modern Physics, Lanzhou 730000, People's Republic of China
[31]Institute of Physics and Technology, Peace Avenue 54B, Ulaanbaatar 13330, Mongolia
[32]Instituto de Alta Investigación, Universidad de Tarapacá, Casilla 7D, Arica, Chile
[33]Jilin University, Changchun 130012, People's Republic of China
[34]Johannes Gutenberg University of Mainz, Johann-Joachim-Becher-Weg 45, D-55099 Mainz, Germany
[35]Joint Institute for Nuclear Research, 141980 Dubna, Moscow region, Russia
[36]Justus-Liebig-Universitaet Giessen, II. Physikalisches Institut, Heinrich-Buff-Ring 16, D-35392 Giessen, Germany
[37]Lanzhou University, Lanzhou 730000, People's Republic of China
[38]Liaoning Normal University, Dalian 116029, People's Republic of China
[39]Liaoning University, Shenyang 110036, People's Republic of China
[40]Nanjing Normal University, Nanjing 210023, People's Republic of China
[41]Nanjing University, Nanjing 210093, People's Republic of China
[42]Nankai University, Tianjin 300071, People's Republic of China
[43]National Centre for Nuclear Research, Warsaw 02-093, Poland
[44]North China Electric Power University, Beijing 102206, People's Republic of China
[45]Peking University, Beijing 100871, People's Republic of China
[46]Qufu Normal University, Qufu 273165, People's Republic of China
[47]Shandong Normal University, Jinan 250014, People's Republic of China
[48]Shandong University, Jinan 250100, People's Republic of China
[49]Shanghai Jiao Tong University, Shanghai 200240, People's Republic of China
[50]Shanxi Normal University, Linfen 041004, People's Republic of China
[51]Shanxi University, Taiyuan 030006, People's Republic of China
[52]Sichuan University, Chengdu 610064, People's Republic of China
[53]Soochow University, Suzhou 215006, People's Republic of China
[54]South China Normal University, Guangzhou 510006, People's Republic of China
[55]Southeast University, Nanjing 211100, People's Republic of China
[56]State Key Laboratory of Particle Detection and Electronics, Beijing 100049, Hefei 230026, People's Republic of China
[57]Sun Yat-Sen University, Guangzhou 510275, People's Republic of China
[58]Suranaree University of Technology, University Avenue 111, Nakhon Ratchasima 30000, Thailand
[59]Tsinghua University, Beijing 100084, People's Republic of China
[60a]Turkish Accelerator Center Particle Factory Group, Istinye University, 34010, Istanbul, Turkey
[60b]Near East University, Nicosia, North Cyprus, 99138, Mersin 10, Turkey
[61]University of Chinese Academy of Sciences, Beijing 100049, People's Republic of China
[62]University of Groningen, NL-9747 AA Groningen, The Netherlands
[63]University of Hawaii, Honolulu, Hawaii 96822, USA
[64]University of Jinan, Jinan 250022, People's Republic of China
[65]University of Manchester, Oxford Road, Manchester, M13 9PL, United Kingdom

[66]University of Muenster, Wilhelm-Klemm-Strasse 9, 48149 Muenster, Germany
[67]University of Oxford, Keble Road, Oxford OX13RH, United Kingdom
[68]University of Science and Technology Liaoning, Anshan 114051, People's Republic of China
[69]University of Science and Technology of China, Hefei 230026, People's Republic of China
[70]University of South China, Hengyang 421001, People's Republic of China
[71]University of the Punjab, Lahore-54590, Pakistan
[72a]University of Turin and INFN, University of Turin, I-10125, Turin, Italy
[72b]University of Eastern Piedmont, I-15121, Alessandria, Italy
[72c]INFN, I-10125, Turin, Italy
[73]Uppsala University, Box 516, SE-75120 Uppsala, Sweden
[74]Wuhan University, Wuhan 430072, People's Republic of China
[75]Xinyang Normal University, Xinyang 464000, People's Republic of China
[76]Yantai University, Yantai 264005, People's Republic of China
[77]Yunnan University, Kunming 650500, People's Republic of China
[78]Zhejiang University, Hangzhou 310027, People's Republic of China
[79]Zhengzhou University, Zhengzhou 450001, People's Republic of China

[a]Also at the Moscow Institute of Physics and Technology, Moscow 141700, Russia.
[b]Also at the Novosibirsk State University, Novosibirsk, 630090, Russia.
[c]Also at the NRC "Kurchatov Institute", PNPI, 188300, Gatchina, Russia.
[d]Also at Goethe University Frankfurt, 60323 Frankfurt am Main, Germany.
[e]Also at Key Laboratory for Particle Physics, Astrophysics and Cosmology, Ministry of Education; Shanghai Key Laboratory for Particle Physics and Cosmology; Institute of Nuclear and Particle Physics, Shanghai 200240, People's Republic of China.
[f]Also at Key Laboratory of Nuclear Physics and Ion-beam Application (MOE) and Institute of Modern Physics, Fudan University, Shanghai 200443, People's Republic of China.
[g]Also at State Key Laboratory of Nuclear Physics and Technology, Peking University, Beijing 100871, People's Republic of China.
[h]Also at School of Physics and Electronics, Hunan University, Changsha 410082, China.
[i]Also at Guangdong Provincial Key Laboratory of Nuclear Science, Institute of Quantum Matter, South China Normal University, Guangzhou 510006, China.
[j]Also at Frontiers Science Center for Rare Isotopes, Lanzhou University, Lanzhou 730000, People's Republic of China.
[k]Also at Lanzhou Center for Theoretical Physics, Lanzhou University, Lanzhou 730000, People's Republic of China.
[l]Also at the Department of Mathematical Sciences, IBA, Karachi 75270, Pakistan.